Ischemia is the prime but not the only cause of hMSC death in tissue engineered constructs in vivo

Authors: Pierre Becquart[1*], Adeline Cambon-Binder[1*], Laurent-Emmanuel Monfoulet[1], Marianne Bourguignon[1], Katleen Vandamme [1,2], Morad Bensidhoum [1], Hervé Petite [1] and Delphine Logeart-Avramoglou [1]

Affiliations:

1: Laboratory of Bioengineering and Bioimaging for Osteo-Articular tissues UMR 7052 CNRS, Univ Paris Diderot, Sorbonne Paris Cité, France

2: Department of Prosthetic Dentistry, Biomat Research Cluster KU Leuven, Leuven, Belgium.

*: These authors equally contributed to this work.

Key words: multipotent stromal cells; in vivo fate; tissue engineering; cell survival; ischemia

Abstract: Local tissue ischemia is a prime cause responsible for the massive cell death in tissue engineered (TE) constructs observed post-implantation. In order to assess the impact of ischemia on the death of implanted human multipotent stromal cells (hMSCs), which have great potential for repairing damaged tissues, we hereby investigated the in vivo temporal and spatial fate of human Luc-GFP-labeled MSCs within fibrin gel/coral scaffolds subcutaneously implanted in nude mice. In vivo bioluminescence imaging monitoring and histological analyses of the constructs tested confirmed the irremediable death of hMSCs over 30 days post-implantation. The kinetics of expression of three hypoxic/ischemic markers (HIF-1α, LDH-A and BNIP3) was also monitored. Our results provided evidence that hMSC located within the core of implanted constructs died faster and predominantly as well as strongly expressed the aforementioned ischemic markers. In contrast, cells located in the outer regions of TE constructs were reperfused by neovascularization and were still viable (as evidenced by their ex-vivo proliferative potential) at day 15 post-implantation. These results support the explanation that in the central part of the constructs tested, death of hMSC cells was due to ischemia, whereas in the periphery of these constructs, cell death was due to another mechanism that needs to be elucidated.

Introduction:

Tissue engineering (TE) aims at regenerating functional tissues by combining cells with a supporting substrate. Owing to their expansion potential, ability to adopt different phenotypes, paracrine effects, and immune-modulatory properties, multipotent stromal cell (MSC) 1 represent a promising cell population for repairing damaged tissues such as bone 2,3, cartilage 4, kidney, muscle, skin, neural, and cardiac tissues 5,6. However, the efficacy of MSC-based TE in experimental and clinical studies has been less than optimal. For example, when addressing the repair of massive bone defects in a clinically relevant segmental bone defect model, the osteogenic ability of tissue constructs was superior to the one of scaffold alone but remained inferior to that of autologous bone grafts, the benchmark for bone repair 7.

The underlying reasons for the limited efficacy of tissue constructs are not yet fully understood but one of them is the massive disappearance of transplanted cells during the first weeks post-implantation. Indeed, using different cellular and molecular labeling approaches to track implanted cells, several researchers reported the loss (from 70 to 100%) of either animal- or human-derived MSCs loaded into scaffolds and implanted either subcutaneously 8-10 or into skeletal bone defects 11-13 in rodent models within the first month after implantation. Although the mechanisms or biological cascade behind such extensive loss of implanted cells remains poorly understood, the hostile environment that MSC faced when loaded on synthetic material constructs devoid of pre-existing vascular network 14 is considered as a prime reason. Upon implantation, MSC encounter an ischemic environment of low oxygen tension and nutrient deprivation that could lead to their massive death in situ 15. However, information regarding the cellular responses to the ischemic stress is crucially lacking in the TE field. For these reasons, the aim of the present study was to assess the impact of ischemia on the loss of human MSC implanted in vivo. Because the intensity of the ischemic state that individual cells face varies with both their location throughout the construct (especially their distance from blood capillaries) and the post-implantation time, we hereby investigated the in vivo hMSCs fate at different levels of depth within TE constructs and at early, mid- and late post-implantation time points.

A human MSC line 16 was transduced using lentiviral vectors encoding both firefly luciferase and eGFP reporter genes under the control of a constitutively active promoter. Cell viability, after the labeled cells were seeded onto fibrin gel/coral ceramic scaffolds and implanted subcutaneously in nude mice, was monitored in each cell construct non-invasively by bioluminescence imaging over a period of 30 days. Because an excessively large number of cells within the scaffolds may worsen the ischemic conditions at the implantation site, the effect of the number of transplanted cells in their survival was particularly addressed. To further assess the metabolic stress induced by the ischemic environment, immunohistochemistry analyses were performed to establish maps of either implanted cells, apoptotic cells or hypoxia-responsive cells via the expression of Hypoxia-inducible factor-1 (HIF-1α□□ and of two downstream proteins: the lactate deshydrogenase-A (LDH-A) and Bcl-2/adenovirus E1B 19 kDa-interacting protein 3 (BNIP3). LDH-A is a marker of an anaerobic environment since this enzyme converts pyruvate (derived from glucose) to lactate through anaerobic glycolysis 17. BNIP3 is a marker of cell nutrient stress 18 and is implicated in the induction of autophagy 19,20. In the present study, the progression of the expression of these markers was monitored within specific regional zones defined

within cell constructs retrieved at early, mid- and late post-implantation time points.

Materials and Methods:

Cell transduction

A human immortalized multipotent stromal line (hMSC line SV56 16), which expresses characteristics of human MSCs, was used in the present study. The hMSC SV56 line expresses the stromal marker (48% of Stro1 positive cells), and CD105 (SH2) and CD73 (SH3), two mesenchymal cell markers (more than 90% positive cells) 16. The multipotential property of the hMSC line SV56 was established by the ability to differentiate towards osteogenic, adipogenic and chondrogenic lineages (Supplementary Figure 1).

HMSC line SV56 line was genetically modified using a bicistronic lentiviral vector encoding firefly luciferase (fLuc) and enhanced green fluorescent protein (eGFP; pCHMWS-fLuc-T2A-eGFP). The T2A sequence ensured efficient coexpression of both reporter genes 21,22. The LV-fLuc-T2A-eGFP vectors were obtained from Dr. A. Ibrahimi (Katholieke Universiteit, Leuven, Belgium). The hMSC were cultured in alpha-Modified Eagle Medium (α-MEM; Sigma) supplemented with 10% fetal calf serum (FCS), penicillin (100 U/ml), and streptomycin sulfate (100 µg/ml) (all chemicals from the PAA Laboratories, France) under standard cell culture conditions. The cells were transduced with lentiviruses (at the concentration of 0.64 pg of p24 viral coat protein per cell) as previously described 23. The efficiency of transduction was assessed by quantifying fluorescent and bioluminescent signals and comparing them to those obtained from non-transfected cells. Flow cytometry analysis of GFP positive cells provided evidence that 88% of the transduced cells (designed as Luc-GFP-hMSC) were transduced. Luciferase expression in Luc-GFP-hMSC was linear with the cell number (ranging from 10 to 106 cells; $r^2 = 0.98$). Upon expansion, both Luc-GFP-hMSC and hMSC displayed similar proliferation rates (doubling times at 2.43±0.46 and 2.36±0.04 days for transduced and non-tranduced hMSC, respectively). When cultured under expansion conditions over 5 passages (10 doubling populations), the Luc-GFP-hMSC luciferase-related activity was constant.

Preparation of cell-containing constructs

Luc-GFP-hMSC were seeded on natural Porites coral (Biocoral®) particles (600 to 1,000 µm diameter) donated by Inoteb, Inc. (Levallois-Perret, France). This material consisted of 99% calcium carbonate in the form of aragonite, had open, communicating pores with a mean diameter of 100-300 µm, and a porosity of 49% 24,25. The proliferative potential of the hMSC SV56 cells seeded into coral scaffold was checked and was confirmed in vitro (Supplementary Figure 2). Prior to cell seeding, aliquots of 40 mg of Porites coral particles were sterilized by autoclaving. For the study of the in vivo monitoring of the survival of implanted cells by bioluminescence imaging, four different densities of Luc-GFP-hMSC (suspended in 100 µl α-MEM containing 10% FCS, antibiotics, and 25 mM HEPES), were tested and delivered to each coral particle group: specifically, 5x10^6 (n=5 constructs), 1x10^6 (n=6), 1x10^5 (n=6) and 1x10^4 (n=6) cells per cell construct. For the immunohistological studies of the constructs either non-implanted (day 0) or explanted at day 6, day 15 and day 30 post-implantation, only three cell seeding densities were tested (specifically, 1x10^6, 1x10^5 and 1x10^4 cells per cell construct; n=5 constructs for each case). After two hours of incubation at 37°C, the supernatant (100 µl) was discarded and the particles were embedded in a fibrin gel (Tissucol®, Baxter) as previously described 26. Briefly, first 100 µl of fibrinogen (18 mg/ml), and then 40 µl of thrombin (100 IU/ml) were added to the cell-seeded scaffold particles. The constructs used in the present study had a diameter of 0.5 cm. These cell constructs were then maintained in 2 ml of standard growth medium at 37°C overnight. Cells contained in the supernatant of each construct were counted using a Coulter counter (Beckman-Coultronics). The results confirmed that the cells were properly loaded on the constructs tested (data not shown). Unseeded scaffolds served as negative controls. To control the efficacy of cell seeding, each construct was imaged (as described in the "In vivo non-invasive bioluminescence imaging (BLI) and image analysis" section) in vitro just before implantation in animals. Analysis of the BLI images of Luc-GFP-hMSC-containing constructs provided evidence of a linear relationships ($r^2 = 0.98$) between the level of detected photons and the number of cells present in each construct (Supplementary Figure 3).

In vivo implantation

Ten-week-old female nude mice were obtained from Janvier (Legenest-Saint-Isle, France) and handled according to the "European Guidelines for Care and Use of Laboratory Animals" (EEC Directives 86/609/CEE of 24.11.1986). All experimental animal procedures conducted in the present study were approved by the Ethics Committee on Animal Research of Lariboisiere/Villemin, Paris, France. One day after preparation of the cell-containing constructs (as described in the "Preparation of cell-containing constructs" section), each mouse was anesthetized by intra-peritoneal injection of 100 mg/kg ketamine (Ketalar®, Panpharma, Virbach) and 10 mg/kg xylazine (Rompun® 2%, Bayer). The skin of the animals was prepared for surgery using povidone-iodine (Bétadine®). Two symetrical incisions (0.5 cm in length) were made on the back of each mouse on both sides of the lumar spine and subcutaneous pouches were created. The cell-containing constructs of interest to the present study were carefully inserted in each pouch (two per mouse). The soft tissues at the implantation sites were then closed with two interrupted non-resorbable sutures. For the in vivo monitoring of implanted cell survival, the animals were then imaged (as described in the "In vivo non-invasive bioluminescence imaging (BLI) and image analysis" section) twice a week before they were sacrificed using a pentobarbital overdose (Dolethal®, Vetoquinol) at 30 days post-implantation. For the immunohistological studies, sets of animals were sacrified at day 6 and 15 post-implantation. The constructs were explanted at that time and prepared for histological analysis as described in the "Histology / immunohistology" section.

In vivo non-invasive bioluminescence imaging (BLI) and image analysis

The mice tested in the present study were imaged twice a week during the 30-day post-implantation period as previously described 23. For this purpose, the mice were anesthetized by inhaling isoflurane. Thereafter, 50 µl of D-luciferin (20 mg/ml in PBS) were locally injected at each implantation site. After 10 minutes (and while still inhaling isoflurane), the animals were placed in the prone position inside the detection chamber of a bioluminescence imaging system (Ivis Lumina II□, Caliper Life Sciences) and were imaged. Standard regions of interest (ROI) surrounding each implant were manually delineated on the bioluminescence images and the photon flux emitted by each

construct was quantified using the Living Image® 3.1 software (Caliper Life Science).

Histology / immunohistology

At the end of the implantation time (specifically, 6, 15, and 30 days post-implantation), the implants were explanted and fixed in 4% paraformaldehyde (pH 7.4) for 36 hours, decalcified in EDTA (14.5% w/v) at 4°C for one week, and embedded in paraffin. A set of non-implanted cell constructs were prepared in parallel (as described in the "Preparation of cell-containing constructs" section) and were processed for histology (on day 0). Sequential sections (each 5 µm thick) were either stained with hematoxylin-eosin-safranin (HES) or processed for immunodetection (for GFP, HIF-1α, LDHA, BNIP3) or for TUNEL labelling. For immuno-detection, tissue sections were paraffin dewaxed, rehydrated, and rinsed with 0.1M phosphate saline buffer (PBS; pH 7.4). These tissue sections were then pre-treated either in a citrate buffer (0.01 mM, pH=6) at 95°C for 20 min, for subsequent HIF-1α, LDHA and BNIP3 detection, or in a proteolytic enzyme solution (Dako, Glostrup, Denmark) at 37°C for 20 min for subsequent GFP detection. Cell membranes were permeabilized using 0.3% Triton X-100 for 15 min; the endogenous peroxidase activity was inhibited by addition of peroxidase block (Kit Envision+, Dako) and the non-specific binding sites were blocked using Protein Block (Dako). The tissue sections thus prepared were subsequently incubated in a humidified chamber in primary antibody (polyclonal rabbit anti-GFP 1/200 (ClonTech), polyclonal rabbit anti-HIF-1α 1/100 (Novus biological), polyclonal rabbit anti-BNIP3 1/400 (Abcam), and in polyclonal rabbit anti-LDHA 1/1,000, (Abcam)) for 1 hour, incubated with Labelled Polymer-HRP Anti-Rabbit antibody (Envision+ Kit, Dako K4011) for 30 min, and visualized using the DAB chromogen in the dark for 5 min (Envision+ Kit, Dako K4011). Tissue sections from human epidermis biopsies, and tissue sections cell-containing constructs processed without the primary antibody were used as negative controls. Immunostaining for the HIF-1α and BNIP3 proteins on human epidermis samples were undetectable while the LDH-A protein was only detected in the basal layer (Supplementary Figure 4). Immunostaining for the HIF-1α, LDH-A and BNIP3 proteins on tissue sections from unseeded constructs explanted at day 6 and day 15 post-implantation was also performed in order to assess expression of ischemic markers on cells coming from the invading host tissue as well as to determine any cross reaction of primary antibodies with scaffold components. The images obtained form these analyses showed the absence of cell labelling for the three proteins tested at both explantation time points. It should be noted that the anti-HIF-1α staining on the construct explanted at day 6 exhibited strong non-specific staining of the fibrin gel (Supplementary Figure 5).

Detection of apoptotic cells, based on labeling of DNA strand breaks (TUNEL labeling), was performed using the "In situ cell-death detection kit" (Roche) and following the manufacturer's protocol. Briefly, tissue sections were paraffin dewaxed, rehydratated, permeabilised in a 0.1% sodium citrate/0.1% Triton X-100 solution for 8 min, then incubated with labeling TUNEL (fluorescein-dUTP in 50 µl per section) reaction mix, in the dark at 37°C for 1 hour. After rinsing with phosphate buffer three times, the labelled specimens were maintained in 50 µl of Converter-AP (anti-fluorescein-AP conjugate) in a humidified chamber at 37° C for 30 min, rinsed three times with phosphate buffer, treated with 100 µl BCIP/NBT Substrate (Sigma Aldrich), and again maintained in the dark at 20° C for 10 min. This labeling process was terminated by rinsing pertinent specimens with phosphate buffer three times. Specimens treated with 1 U/mL of DNAse (Invitrogen) were used as the positive control (Figure 3; insert).

Histological analyses

To aid histological and immunohistochemical examination, regional analysis zones were defined within the implants, and the progression of events such as cell apoptosis and cell expression of hypoxic/ischemic markers were monitored within these zones. For TUNEL, anti-GFP, anti-HIF-1α, anti-LDHA and anti-BNIP3 labeling, two stained sections from each scaffold (chosen at two different locations in the middle of each construct) were digitalized using a slide scanner (ScanScope TM, Aperio , Vista USA). Images were collected using the TRIBVN ICS software (TRIBVN, Chatillon, France), then exported (*.tiff format) into photo imaging software (Coral Paint Shop Pro X) for analysis. For the GFP- and TUNEL positive cells analyses, the periphery of each implant on the images of each tissue section of interest to the present study was delineated, then two other lines were drawn concentrically at a distance of 500 µm and the other at 1,000 µm from, but along, the periphery of each section; in this fashion, outer, in-between and inner areas were delineated that represented 40%, 30% and 30% of the whole construct surface, respectively. The GFP- and TUNEL positive cells in each of these areas were then counted. For the HIF-1α, LDHA, BNIP3 positive cells analyses, three different fields located in the outer and inner area of each construct were examined (at 40X magnification), and the number of labelled cells was counted and normalized over the total number of cells (both labeled and unlabelled corresponding to more than 100 cells) counted within the same field.

Ex vivo analyses

To further assess the viability of implanted cells, constructs seeded with 1x106 cells (n=8 constructs) were explanted after 2, 6 and 15 days post-implantation. Cells (both surviving hMSC and invading host cells) from each explant were isolated by enzymatic digestion (via incubation in a solution of collagenase type I 1% (w/v) and type IV 1% (w/v) in HBSS medium at 37°C for 30 min) of the constructs then seeded onto 2 wells of a 6 well-plate. Twenty-four hours after cell seeding, the cell cultures were washed twice with PBS (to eliminate remnant debris) and the cells were cultured in standard tissue culture medium. The growth kinetics of the explanted Luc-GFP hMSC cells were monitored non-invasively by BLI after addition of 360 µg/ml luciferin substrate every 2 or 3 days after cell seeding till the cells reached confluence. To ensure that the presence of murine host cells do not impede the hMSC proliferation, and since the hMSC line SV56 cells contained the neomycin gene 16, these cells were treated with G418 (400µg/ml).

Statistical analyses

Numerical results were reported as average ± standard error of the mean (SEM). For in vivo experiments, multiple samples were analyzed for each group, specifically, n=6 constructs for the time course study and n=5 constructs for the histological analyses. Statistical analyses were conducted using the Statgraphics centurion version XV.2 (Statpoint, Inc., Herdon, VA, USA). Quantitative data from in vivo BLI signals were analyzed by two-way analysis of variance (ANOVA). The nonparametric Mann-Withney U test was used to analyze data from two independent samples. For all analyses, differences at $p \leq 0.05$ were accepted to be statistically significant.

Results

Independent of cell seeding densities, implanted hMSC died massively

The BLI signal from each implanted construct was monitored twice-a-week over the 30-day period of the study (Fig 1A). In order to compare cell survival as a function of various cell-seeding densities for each construct tested, photon fluxes were normalized with respect to the signal acquired at the beginning (day 1-acquisition) of the in vivo period (Fig 1B). The cell survival rate was significantly ($p<0.05$) higher within the constructs seeded with 1x106 cells compared to the results obtained with the other cell-densities tested till day 30 p ost-implantation. It should be noted that half of the implants seeded with 1x106 cells exhibited an increased BLI signal over the first 6 days post-implantation. No difference in cell survival rates was observed for the other cell-densities tested during that time period. After day 6, continuous decrease in the luminescence signal from all implanted cell-containing constructs was observed; as a result, less than 1% of the initial cell numbers for all constructs tested remained at 30 days post-implantation.

This loss of hMSCs upon implantation was confirmed by the results obtained from GFP immunostaining of sections from cell-containing constructs either non-implanted (day 0) or explanted at days 6, 15 and 30 post-implantation. Before implantation, the numbers of quantified GFP-cells were, however, underestimated because most of the seeded cells were closely adhered onto the scaffold surface and were not distributed within the fibrin gel as much as those observed post-implantation rendering the individual cell counting difficult. After implantation, the number of histologically visualized GFP-labelled cells was highest at day 6 post-implantation but decreased dramatically at day 15 and day 30 post-implantation. Only the constructs seeded with 1x106 cells still contained a significant ($p<0.01$) number of GFP-labelled cells at day 15 post-implantation but few of the GFP expressing cells remained at the end the study period, that is 30 days post-implantation (Fig 2A). Discrepancy was, however, noted between the results obtained from BLI detection and those from GFP cell counting at day 30 (less than 1% cell survival vs 25% survival, respectively). Such a discrepancy could be due to the fact that BLI detection assesses the viability of implanted cells dynamically because of the short half-life (approximately 2-4 h) of the luciferin substrate; in contrast GFP (with half-life of several days) is a stable protein that may remain immunodetectable for few days after cell death.

To further understand the fate of hMSC in the constructs seeded with 1x106 cells (the ones with the optimal in vivo viability), the number of apoptotic cells was also quantified on pertinent explants sections using TUNEL staining (Fig 2B). Although no sign of cell apoptotis was observed at the time of implantation of the cell constructs, the number of TUNEL positive cells increased at day 6 post-implantation, peaked at day 15 post-implantation (Fig 2B), and was statistically different from the results obtained from the respective unseeded control group (which represented the average rate of apoptotic cells from the invading host tissue); at day 15 time point, the apoptotic cells represented 45% of the GFP-positive cells counted in the same construct section (Fig 2B; insert). The number of TUNEL-positive cells decreased at day 30 post-implantation, but still represented 57% of the GFP-positive cells.

Taken together, these data provided evidence that, although the seeding density of hMSCs affected cell survival at early times post-implantation, long-term viability of the implanted cells in TE constructs irremediably declined over time at all cell seeding densities tested; moreover, cell death by apoptosis peaked, and remained elevated after day 15 post-implantation.

Implanted hMSC died in the inner part of the construct first

In order to assess the impact of cell location within the TE constructs on the death of implanted cells, regions (specifically, outer, in-between, and inner areas) were defined within the explant sections, and the progression of events (such as disappearance of GFP-expressing cells and cell apoptosis) were monitored within each one of these zones.

GFP-labelled cells on individual sections from constructs seeded with 1x106, 1x105 and 1x104 cells were histologically visualized and quantified; the results from constructs seeded with 1x106 cells are representative of this analysis and are shown on Fig 3A, B, C and D. Analysis of cell-containing but non implanted constructs (day 0) revealed that the seeded cells adhered onto the coral scaffold (Fig 3A) and were uniformly distributed throughout the examined constructs as evidenced by the similar percentage of GFP-labelled cells present in each area (Fig 3H). At day 6 post-implantation, the GFP-positive cells had migrated within the fibrin gel (Fig 3B) and were uniformly distributed throughout the sections for all cell seeding densities tested (Fig 3H). At day 15 post-implantation, the remaining GFP-cells from constructs seeded with 1x106 and 1x105 cells were still evenly distributed throughout the respective constructs while cells from constructs seeded with 1x104 cells were located exclusively in the outer area ($p<0.05$). After 30 days, there were no GFP-expressing cells of constructs seeded with 1x105 cells in both the inner and in-between areas ($p<0.05$); in contrast, GFP-expressing cells of constructs seeded with 1x106 cells were still present in the core of the implant but displayed a necrotic/apoptotic aspect ($p<0.05$).

Observation and analysis of TUNEL-stained sections from the constructs seeded with 1x106 cells confirmed that the apoptotic cells were mainly located in the core of the implant at all explantation time points tested (Fig 3E, F and G). Specifically, 47-59 % and 30-40% of the apoptotic cells were present in the inner and in-between areas, respectively (Fig 3I). In contrast, a small number of apoptotic cells was present in the outer area at all post-implantation time points tested.

Altogether, these results provided evidence that implanted hMSC died faster, and predominantly, when located in the inner part of the constructs; this effect was enhanced when these cells were seeded at low (1x105 and 1x104) cell density.

hMSC seeded in constructs expressed ischemic markers in vivo

The prevalence of dead hMSC in the core of the constructs of interest of the present study strongly suggested that ischemia is the main cause responsible for the observed loss of implanted cells. To validate that the implanted cells were exposed to ischemia, expressions of three ischemia-induced markers, specifically, HIF-1α (hypoxia), LDH-A (anaerobic metabolism) and BNIP3 (autophagy), were monitored on explants sections from the constructs seeded with 1x106 cells. At day 0, hMSCs seeded in the constructs expressed these three markers but at different levels of intensity. At that time, HIF-1α expression was mainly cytoplasmic

but nuclear staining was observed in less than 10 % of these cells (Fig 4A and 4B). In contrast, all cells within the constructs exhibited strong LDH-A (Fig 4C and 4D) and BNIP3 (Fig 4E and 4F) protein expression at the cytoplasmic level. After implantation, the three ischemic markers tested were still expressed up to day 6 post-implantation: 70-85% of the cells in the construct displayed an HIF-1α cytoplasmic staining while nuclear staining appeared simultaneously with an accentuated cytoplasmic expression (Fig 4A and 4B). Similarly, 74-90% of the cells expressed LDH-A (Fig 4C and 4D). Expression of the autophagic marker decreased with cell location since 26% of the cells within the outer area and 56% of the cells in the core of the construct exhibited cytoplasmic BNIP3 labelling ($p<0.05$). Expression of cell three ischemic markers tested strongly decreased after 15 days (Fig 4B, 4D and 4F) and disappeared at 30 days post-implantation (data not shown). Immunostaining of tissue sections from unseeded constructs explanted 6 and 15 days post-implantation was also performed to assess the expression of ischemic markers by the invading host tissue (Supplementary Figure 5). The absence of specific cell labelling for either the HIF-1α or LDHA or BNIP3 proteins provided evidence that the host cells did not express the ischemic markers; expression of the observed ischemic markers was, therefore, related to the implanted cells.

Comparison of stainings for each ischemic marker by cells present in the inner and outer parts of the constructs evidenced that the intensity was stronger, and the frequency was higher, in areas located deeper in the construct. The numbers of HIF-1α-labelled cells at both the cytoplasmic and nuclear levels in the inner construct area were higher than those present in the outer area at all time points tested (Fig 4B). At day 6 and 15, staining of LDH-A and BNIP3, respectively, attenuated in cells located in the outer area but remained high in cells located in areas still containing remnant fibrin gel in the core of the construct (Fig 4C and 4F).

These results provided evidence that hMSCs seeded in the constructs tested expressed the hallmarks of ischemia before and after their implantation. In addition, these data also provided evidence that hMSC experienced two distinct levels of ischemia depending where they were located in the outer or in the inner part of the construct; the ischemic stress in the core of the constructs was the strongest.

hMSC in the constructs tested remained viable up to 15 days post-implantation

Histological analysis of specimens stained with HES (Supplementary Figure 6) provided evidence for the development of vascular networks originating at the host tissue that colonized the periphery of the implant (<500 µm of depth) as early as 6 days post-implantation. The vascularisation process continued over time, entirely invaded the outer part of the implanted construct after 15 days and the whole construct after 30 days. At day 15 post-implantation, the outer area (<500µm of depth) displayed the following features: (i) the number of TUNEL-positive cells present in this area was insignificant (Fig 3I); (ii) the number of GFP-positive cells was still high (Fig 3H); and (iii) this area was reperfused (invaded by neovascular networks). However, these remaining hMSC irremediably continued to disappear at later (up to 30 days) time points evidenced by the loss of the respective BLI signal during those times. This result raises the question whether the hMSC remaining at day 15 were still viable or experienced a primary fatal metabolic stress that would lead to their subsequent death. To elucidate this aspect, the proliferative potential of these cells was compared to that of hMSC present in TE constructs at earlier (day 2 and day 6) time points and to hMSC that were not seeded onto scaffolds. TE constructs were explanted after 2, 6 and 15 days post-implantation and cells from each construct were recovered and cultured under standard in vitro tissue culture conditions. The average number of hMSCs recovered from each explant (estimated by the BLI signal emitted 1 day post-seeding and compared to a standard curve of luciferase labelled-hMSC) were 53,000, 123,000 and 10,000 Luc-GFP-MSCs for the TE constructs explanted at day 2, 6 and 15 post-implantation, respectively. The proliferation rates of explanted cells were comparable in all groups tested and exhibited a delay of the exponential phase for the group explanted at day 15 (Fig 5). This delay was explained by the low Luc-GFP hMSC seeding density (less than 10,000 cells/cm²) resulting from their low number recovered from day 15 TE constructs; indeed, a study of cell proliferation starting with different seeding densities demonstrated that non-implanted hMSC seeded at less than 10,000 cells/cm² did not proliferate over a 18-day period of culture (Fig 5 insert). These results provided evidence that hMSCs present in TE constructs for up to 15 days post-implantation were viable and displayed a similar proliferative potential as the non-implanted hMSC cultured under standard (21% O2) cell culture conditions

Discussion:

Massive cell death observed in tissue constructs in vivo is a major impediment to their ultimate biological functionality. Despite the crucial need to better understand the biological and biochemical cascades that lead to such massive cell loss, only few studies that assess the death of implanted progenitor cells in a tissue engineering perspective have been reported in the literature. Local tissue ischemia is considered a prime cause for such accelerated cell mortality but it has never been clearly demonstrated in TE constructs so far. The present study was an attempt to fill this gap of knowledge. Ischemia originates from inadequate vascularisation within implanted constructs; absence of pre-existing vascular networks provokes an environment of low oxygen tension and nutrients as well as growth factors deprivation that implanted cells encounter in constructs; such metabolic stress strongly affects cell survival. In order to assess the impact of ischemia on the loss of implanted hMSC as a function of their location in implanted constructs, we hereby investigated the in vivo temporal and spatial fate of hMSC within a fibrin gel/coral ceramic scaffold in an ectopic mice model. The present study focused on the early (< 30 days) fate of implanted cells. For this reason, assessment of the osteogenic ability of the tested tissue constructs was outside the scope of this study. Fibrin gel was selected and used as the scaffold material because it promotes hMSC adhesion, spreading, as well as the angiogenesis and wound healing processes 26,27. Coral ceramic also promotes cell adhesion, proliferation as well as osteogenic differentiation of bone marrow-derived stem cells 7,28. In the present study, the hMSC SV56 cell adhesion and proliferation on this scaffold was checked and confirmed in vitro. Based on these results, any causal effect of cell loss due to the composite scaffold biomaterial used was excluded. However, because some aspects of the material substrate, such as physicochemical features, size, shape, and porosity may critically affect cell functions pertinent to new tissue formation (including survival of grafted cells), the results of the present study cannot be directly compared to those from studies using another scaffold material.

Foremost, our results confirmed massive death of hMSC distributed in coral particles/fibrin gel constructs over time after subcutaneous implantation in nude mice. The number of viable implanted cells decreased consistently over the 30-day period of the study; as a result less than 1% of the initial viable cell number remained at that time. Our results are in agreement with those by other researchers who reported overall loss when MSC were contained in ceramic scaffolds and implanted either ectopically or orthotopically in rodents 8-10,12,13,29. The reported rate of transplanted cell loss varied (from 70 to 100%) within the first month after implantation. Such variations may be explained by differences in MSC origin (species as well as tissue origin), the number of transplanted cells, the scaffold material used, the anatomical site of implantation and the immune tolerance of the implantation model (syngenic vs xenogenic) 8,10,12,13,29,30. In the present study, we investigated the fate of an immortalized hMSC cell line after ectopic implantation in a xenogenic model. Using the same construct model, we recently examined the fate of primary Luc-GFP mMSC (harvested from Luc-GFP transgenic mice) after implantation in a syngenic model and observed similar massive (> 90%) disappearance of the implanted mMSC over the 3 week-period of implantation (unpublished data). Similar results were reported by Tasso et al.10, and more recently by Boukhechba et al.30, who showed that grafted bone-marrow-derived mouse MSCs did not survive more than 3 weeks after implantation in a syngenic model of ectopic bone regeneration. At this time, however, it is not known whether the short-term cell survival of bone-marrow-derived MSC observed in mice may occur in the clinical milieu in autologous cell-based tissue engineering applications. Direct extrapolation to clinical use/applications needs to take into account the specific properties of human bone-marrow-derived MSCs after autologous implantation.

With the exception of the study by Giannoni et al. 9 who reported a peak of apoptosis (evidenced by TUNEL staining of explant sections) of sheep MSCs (distributed in ceramic/fibrin gel scaffolds) at day 2 post-implantation in a similar nude mouse model, however, none of the other studies clearly proved the death of implanted cells; the studies reported either extinction of the BLI signal from Luc-labelled cells contained in constructs or the disappearance of GFP-labelled cells in constructs but not definitive proof of cell death. In contrast, the present study provided evidence of massive cell death by TUNEL labeling of explanted tissue sections and determined that cell death peaked at 15 days and remained elevated at 30 days post-implantation.

Additionally, the effect of the number of seeded cells on their survival upon implantation was assessed: for all cell densities tested, the long-term viability of hMSC on the TE constructs irremediably declined over time for up to 30 days post-implantation. The present study provided evidence that there is an optimal cell seeding density (specifically, 1x106 cells per construct tested) that resulted in the most "favorable" cell survival during the first week post-implantation. In contrast, either too low (1x104) or too high (5x106) cell-seeding densities in the constructs tested accelerated cell death. Although few, some literature reports provided evidence that seeding MSCs at high densities (more than 1x106 cells) in constructs improved the in vivo viability of these cells 13,29. Several studies reported that grafted MSCs act as trophic factors and secrete several bioactive pro-survival paracrine factors 31-33. In the present study, the constructs that contained low (1x104) cell numbers, displayed sparse GFP cells distributed throughout the implanted constructs suggesting that the amount of secreted paracrine factors by the implanted cells was weak to promote their survival in vivo. On the other hand, the fact that cells seeded at high (5x106) density died at the same rate as those seeded at low (1x104) density, suggests that large numbers of cells within scaffolds may consume fast available nutrients (glucose, and amino acids) as well as oxygen and also contribute to local accumulation of cell metabolic waste products 34. The results of the present study indicated that an optimal cell density must be defined for each type of TE construct in order to maintain cell viability in vivo.

Expression of the hypoxia-regulated HIF1α transcription factor and two of its downstream regulated proteins, specifically, LDH-A and BNIP3, provided evidence that the implanted cells of the present study were exposed to ischemia. Cells seeded in the constructs tested (and cultured for 24 hours under standard tissue culture conditions) experienced hypoxia/ischemia before being implanted in animals (day 0 of the study). Upon implantation, the three ischemic markers tested were highly expressed up to day 6. The high LDH-A levels of cells located in the constructs tested in the present study confirmed the switch-on of anaerobic metabolism resulting from the reduced oxygen environment. Furthermore, the BNIP3 expression results proved induction of a pro-survival autophagic response 19. The three ischemic markers decreased at day 15 and were absent at day 30 post-implantation; in fact, they attenuated with kinetics commensurate with those of the invading host tissue.

We further assessed the fate of grafted cells as a function of their location within the constructs tested and found striking differences between the inner and the outer parts of the construct. In the core (>1,000 μm into the construct depth), cells died faster and predominantly (> 50% of TUNEL positive cells were located in the inner area of the constructs); this result was enhanced when the cells were seeded at the low densities tested. Similarly, the frequency of positive cells and the intensity of staining for each ischemic marker tested increased significantly in areas deeper into the construct. All these results provided evidence that the primary metabolic stress encountered by hMSCs intensified in the core of the constructs tested; this evidence supports the explanation that ischemia (a harsh condition specifically found in areas located deep in the TE constructs) is responsible for the observed massive death of implanted cells in these inner construct areas.

In contrast, in the outer part of the constructs (< 500 μm of depth), few apoptotic cells were present at all post-implantation time points tested, while GFP-positive hMSCs were still present in high numbers up to day 15 post-implantation. At this time point, the outer construct area was invaded by vascular networks originating from the colonizing host tissue, while cell ischemic markers had either strongly weakened or disappeared, indicating that these outer areas were possibly reperfused. Nevertherless, monitoring cell viability (as determined by BLI as well as GFP-positive cell quantification) in the constructs tested provided evidence that the implanted cells irremediably continued to disappear at later time points (up to 30 days) post-implantation resulting in the entire loss of implanted cells from the inner and outer construct areas. To rule out the possibility that the implanted cells experienced a primary fatal metabolic stress that led to their death, hMSC from TE construct explants were recovered and cultured under standard tissue culture conditions in vitro. Similar proliferative rates of hMSC explanted at either day 15 or earlier and of non-implanted hMSC provided evidence regarding the

viability of hMSC in TE constructs up to day 15 post-implantation. Taken together, these observations support the explanation that the disappearance of hMSC cells located in the outer area of implanted TE constructs at later time was due to biochemical process distinct from ischemia.

Several possible explanations could be raised for the observed loss of implanted hMSC after reperfusion. Among them, establishment of blood supply following ischemia reintroduced reactive oxygen species that may cause oxidative cell damage leading to loss of function and/or cell death 35. In addition, the invading vascular networks allow the exchange of molecules and cells of different type between the host and the implant, including immune-reactive effector cells. Although undifferentiated MSC populations have the potential to downregulate the immune response, 36,37, one cannot exclude the possibility that the long-term disappearance of a part of implanted exogenous MSCs originated from activation of the host immune system. In the present study, histological examination of explants indicated the presence of some immune cells (including macrophages, polynuclear and lymphocytes to a lesser extend) located in the host tissue invading the constructs at day 15 and day 30 post-implantation; this situation evoked the occurrence of a weak/moderate inflammatory and immune response against the cell constructs (data not shown). The newly-formed vascular networks could also be the way by which implanted MSCs could leave the scaffold and reach other organs through the SDF-1/CXCR4 axis involved in the homing of MSC to injured tissues 38,39. In a similar ectopic model as the one used in the present study, Tasso et al reported migration of exogenous murine MSC from the construct to the spleen 10. In the present study, the BLI signal (displayed in pseudo-color on BLI images taken over the entire period of implantation) remained strictly localized at the site of the implanted cell construct. Also, intraperitoneal injections of Luciferin substrate were performed in each tested animal at the last (30 days) post-implantation time point in order to check the potential migration of luc-labelled hMSC from the implanted site; the BLI images, however, did not provided evidence of BLI signal from any body part of the mice (data not shown). These observations excluded the possibility of a massive migration of implanted hMSC out of the constructs but not the possibility of sparse migration of hMSC which was not detectable by the BLI assay. Further research is needed in order to provide definitive answers to these issues. Nevertheless, understanding the cause of the death/disappearance of cells in the outer zone of implanted constructs is relevant in the bone TE field; in this case, ectopic new bone in implanted constructs was centripetally formed from the periphery towards the central areas of these constructs 30,40,41; this observation highlights the potential role of MSC located in these peripheral areas for new tissue growth.

Although ischemia appeared to be the prime cause, the results of the present study provided evidence that death/disappearance of implanted hMSC is the result of combined complex biological processes (still not fully understood) that need to be thoroughly elucidated. Strategies to enhance cell survival in vivo need to take into account these different, and perhaps additive, events.

Conclusion

The results of the present study provided evidence that, although the seeding density of hMSCs affected cell survival at early times (<15 days), long-term (30 days post-implantation) viability of the TE constructs tested in vivo irremediably declined over time for all cell densities tested. Ischemia was the prime cause of the massive death of transplanted cells. Soon after cell construct preparation, the seeded hMSC were under ischemia that increased after construct implantation in vivo and intensified in the core of the constructs where cells in great numbers died. Another biological mechanism (that still needs to be elucidated) seemed, however, to be responsible of the death/disappearance of viable implanted hMSC remaining in the outer part of TE constructs once neovascular networks were established. Complete identification of conditions responsible for the death of implanted hMSC in tissue engineered constructs is needed to develop relevant strategies for improving hMSC survival in vivo.

Acknowledgments

The authors gratefully acknowledge Inoteb Inc. (Levallois-Perret, France) for donating the coral scaffolds and Baxter, Inc., for donating the Tissucol® used in the present study. We would also like to thank Dr. R. Vallefuoco for his help with the histological analysis, and Professor R. Bizios for critically reading the manuscript. This project was supported by the French National Research Agency (ANR) through the TecSan program (project GLASSBONE n° 08-TECS-004), by the Centre National de la Recherche Scientifique (CNRS), and by the National French Academy of Medicine (ACB).

Disclosure Statement

The authors declare no competing financial interests

References

1. Charbord P. Bone marrow mesenchymal stem cells: historical overview and concepts. Hum Gene Ther 21, 1045, 2010.
2. Cancedda R, Mastrogiacomo M, Bianchi G, Derubeis A, Muraglia A, Quarto R. Bone marrow stromal cells and their use in regenerating bone. Novartis Found Symp 249, 133, 2003.
3. Logeart-Avramoglou D, Anagnostou F, Bizios R, Petite H. Engineering bone: challenges and obstacles. J Cell Mol Med 9, 72, 2005.
4. Chung C, Burdick JA. Engineering cartilage tissue. Adv Drug Deliv Rev 60, 243, 2008.
5. Leclerc T, Thepenier C, Jault P, Bey E, Peltzer J, Trouillas M, Duhamel P, Bargues L, Prat M, Bonderriter M and others. Cell therapy of burns. Cell Prolif 44 Suppl 1, 48, 2011.
6. Sensebe L, Krampera M, Schrezenmeier H, Bourin P, Giordano R. Mesenchymal stem cells for clinical application. Vox Sang 98, 93, 2010.
7. Viateau V, Guillemin G, Bousson V, Oudina K, Hannouche D, Sedel L, Logeart-Avramoglou D, Petite H. Long-bone critical-size defects treated with tissue-engineered grafts: a study on sheep. J Orthop Res 25, 741, 2007.
8. Dennis JE, Haynesworth SE, Young RG, Caplan AI. Osteogenesis in marrow-derived mesenchymal cell porous ceramic composites transplanted subcutaneously: effect of fibronectin and laminin on cell retention and rate of osteogenic expression. Cell Transplant 1, 23, 1992.
9. Giannoni P, Scaglione S, Daga A, Ilengo C, Cilli M, Quarto R. Short-time survival and engraftment of bone marrow stromal cells in an ectopic model of bone regeneration. Tissue Eng Part A, 2009.
10. Tasso R, Augello A, Boccardo S, Salvi S, Carida M, Postiglione F, Fais F, Truini M, Cancedda R, Pennesi G. Recruitment of a host's osteoprogenitor cells using exogenous mesenchymal stem cells seeded on porous ceramic. Tissue Eng Part A 15, 2203, 2009.
11. Jager M, Degistirici O, Knipper A, Fischer J, Sager M, Krauspe R. Bone healing and migration of cord blood-derived stem cells into a critical size femoral defect after xenotransplantation. J Bone Miner Res 22, 1224, 2007.
12. Degano IR, Vilalta M, Bago JR, Matthies AM, Hubbell JA, Dimitriou H, Bianco P, Rubio N, Blanco J. Bioluminescence imaging of calvarial

bone repair using bone marrow and adipose tissue-derived mesenchymal stem cells. Biomaterials 29, 427, 2008.
13. Geuze RE, Prins HJ, Oner FC, van der Helm YJ, Schuijff LS, Martens AC, Kruyt MC, Alblas J, Dhert WJ. Luciferase labeling for multipotent stromal cell tracking in spinal fusion versus ectopic bone tissue engineering in mice and rats. Tissue Eng Part A 16, 3343, 2010.
14. Liu J, Barradas A, Fernandes H, Janssen F, Papenburg B, Stamatialis D, Martens A, van Blitterswijk C, de Boer J. In vitro and in vivo bioluminescent imaging of hypoxia in tissue-engineered grafts. Tissue Eng Part C Methods 16, 479, 2010.
15. Russ AL, Haberstroh KM, Rundell AE. Experimental strategies to improve in vitro models of renal ischemia. Exp Mol Pathol 83, 143, 2007.
16. Loeuillet C, Bernard G, Remy-Martin J, Saas P, Herve P, Douay L, Chalmers D. Distinct hematopoietic support by two human stromal cell lines. Exp Hematol 29, 736, 2001.
17. Firth JD, Ebert BL, Ratcliffe PJ. Hypoxic regulation of lactate dehydrogenase A. Interaction between hypoxia-inducible factor 1 and cAMP response elements. J Biol Chem 270, 21021, 1995.
18. Levine B. Eating oneself and uninvited guests: autophagy-related pathways in cellular defense. Cell 120, 159, 2005.
19. Bellot G, Garcia-Medina R, Gounon P, Chiche J, Roux D, Pouyssegur J, Mazure NM. Hypoxia-induced autophagy is mediated through hypoxia-inducible factor induction of BNIP3 and BNIP3L via their BH3 domains. Mol Cell Biol 29, 2570, 2009.
20. Scarlatti F, Granata R, Meijer AJ, Codogno P. Does autophagy have a license to kill mammalian cells? Cell Death Differ 16, 12, 2009.
21. Deroose CM, Reumers V, Gijsbers R, Bormans G, Debyser Z, Mortelmans L, Baekelandt V. Noninvasive monitoring of long-term lentiviral vector-mediated gene expression in rodent brain with bioluminescence imaging. Mol Ther 14, 423, 2006.
22. Ibrahimi A, Vande Velde G, Reumers V, Toelen J, Thiry I, Vandeputte C, Vets S, Deroose C, Bormans G, Baekelandt V and others. Highly efficient multicistronic lentiviral vectors with peptide 2A sequences. Hum Gene Ther 20, 845, 2009.
23. Logeart-Avramoglou D, Oudina K, Bourguignon M, Delpierre L, Nicola MA, Bensidhoum M, Arnaud E, Petite H. In vitro and in vivo bioluminescent quantification of viable stem cells in engineered constructs. Tissue Eng Part C Methods 16, 447, 2010.
24. Guillemin G, Meunier A, Dallant P, Christel P, Pouliquen JC, Sedel L. Comparison of coral resorption and bone apposition with two natural corals of different porosities. J Biomed Mater Res 23, 765, 1989.
25. Guillemin G, Patat JL, Fournie J, Chetail M. The use of coral as a bone graft substitute. J Biomed Mater Res 21, 557, 1987.
26. Bensaid W, Triffitt JT, Blanchat C, Oudina K, Sedel L, Petite H. A biodegradable fibrin scaffold for mesenchymal stem cell transplantation. Biomaterials 24, 2497, 2003.
27. Janmey PA, Winer JP, Weisel JW. Fibrin gels and their clinical and bioengineering applications. J R Soc Interface 6, 1, 2009.
28. Petite H, Viateau V, Bensaid W, Meunier A, de Pollak C, Bourguignon M, Oudina K, Sedel L, Guillemin G. Tissue-engineered bone regeneration. Nat Biotechnol 18, 959, 2000.
29. Olivo C, Alblas J, Verweij V, Van Zonneveld AJ, Dhert WJ, Martens AC. In vivo bioluminescence imaging study to monitor ectopic bone formation by luciferase gene marked mesenchymal stem cells. J Orthop Res 26, 901, 2008.
30. Boukhechba F, Balaguer T, Bouvet-Gerbettaz S, Michiels JF, Bouler JM, Carle GF, Scimeca JC, Rochet N. Fate of bone marrow stromal cells in a syngenic model of bone formation. Tissue Eng Part A 17, 2267, 2011.
31. Kinnaird T, Stabile E, Burnett MS, Shou M, Lee CW, Barr S, Fuchs S, Epstein SE. Local delivery of marrow-derived stromal cells augments collateral perfusion through paracrine mechanisms. Circulation 109, 1543, 2004.
32. Kinnaird T, Stabile E, Burnett MS, Lee CW, Barr S, Fuchs S, Epstein SE. Marrow-derived stromal cells express genes encoding a broad spectrum of arteriogenic cytokines and promote in vitro and in vivo arteriogenesis through paracrine mechanisms. Circ Res 94, 678, 2004.
33. Chen L, Tredget EE, Wu PY, Wu Y. Paracrine factors of mesenchymal stem cells recruit macrophages and endothelial lineage cells and enhance wound healing. PLoS One 3, e1886, 2008.
34. Muschler GF, Nakamoto C, Griffith LG. Engineering principles of clinical cell-based tissue engineering. J Bone Joint Surg Am 86-A, 1541, 2004.
35. Ryter SW, Kim HP, Hoetzel A, Park JW, Nakahira K, Wang X, Choi AM. Mechanisms of cell death in oxidative stress. Antioxid Redox Signal 9, 49, 2007.
36. Le Blanc K, Ringden O. Mesenchymal stem cells: properties and role in clinical bone marrow transplantation. Curr Opin Immunol 18, 586, 2006.
37. Uccelli A, Moretta L, Pistoia V. Mesenchymal stem cells in health and disease. Nat Rev Immunol 8, 726, 2008.
38. Bensidhoum M, Chapel A, Francois S, Demarquay C, Mazurier C, Fouillard L, Bouchet S, Bertho JM, Gourmelon P, Aigueperse J and others. Homing of in vitro expanded Stro-1- or Stro-1+ human mesenchymal stem cells into the NOD/SCID mouse and their role in supporting human CD34 cell engraftment. Blood 103, 3313, 2004.
39. Fong EL, Chan CK, Goodman SB. Stem cell homing in musculoskeletal injury. Biomaterials 32, 395,
40. Cooper LF, Harris CT, Bruder SP, Kowalski R, Kadiyala S. Incipient analysis of mesenchymal stem-cell-derived osteogenesis. J Dent Res 80, 314, 2001.
41. Kruyt MC, Dhert WJ, Oner FC, van Blitterswijk CA, Verbout AJ, de Bruijn JD. Analysis of ectopic and orthotopic bone formation in cell-based tissue-engineered constructs in goats. Biomaterials 28, 1798, 2007.

Corresponding author:
Dr Delphine LOGEART-AVRAMOGLOU, PhD
Laboratory of Bioengineering and Biomechanics for Bone and Articulations; UMR 7052, CNRS, Paris Diderot University, Sorbonne Paris-Cité, 10 avenue de Verdun 75010 Paris, France
Phone number: +33 1 57 27 85 63
E-mail: delphine.logeart@univ-paris-diderot.fr

To cite this article:
Becquart P, Cambon-Binder A, Monfoulet LE, Bourguignon M, Vandamme K, Bensidhoum M, Petite H, Logeart-Avramoglou D. Ischemia is the prime but not the only cause of human multipotent stromal cell death in tissue-engineered constructs in vivo. Tissue Eng Part A. 2012; 18(19-20):2084-94. doi: 10.1089/ten.TEA.2011.0690.

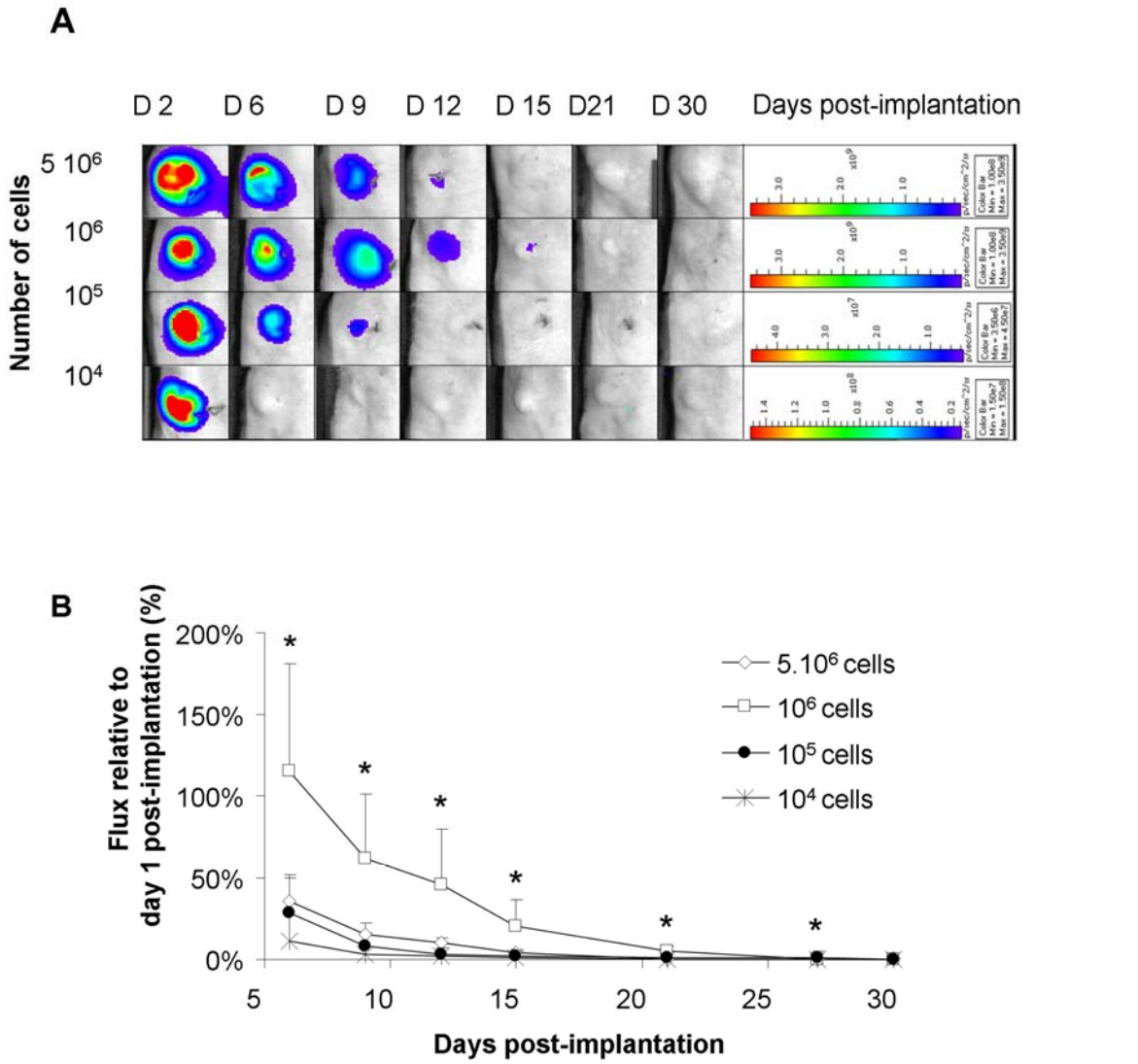

Figure 1: In vivo BLI monitoring of viability of cells in the constructs tested provided evidence of the massive death of implanted hMSC-Luc-GFP at all cell seeding densities tested over 30 days of implantation. (A) Representative BLI images of cell-containing constructs subcutaneously implanted in nude mice. The rainbow pseudocolor scales were adjusted in all images for each cell seeding density group tested. (B) Photon fluxes (normalized to those obtained at day 1 post-implantation for each construct tested) were plotted versus days post-implantation. $p < 0.001$ (two-ways ANOVA); * $p < 0.05$ for the constructs seeded with 1x106 cells compared to constructs seeded with other cell densities (Mann-Whitney test).

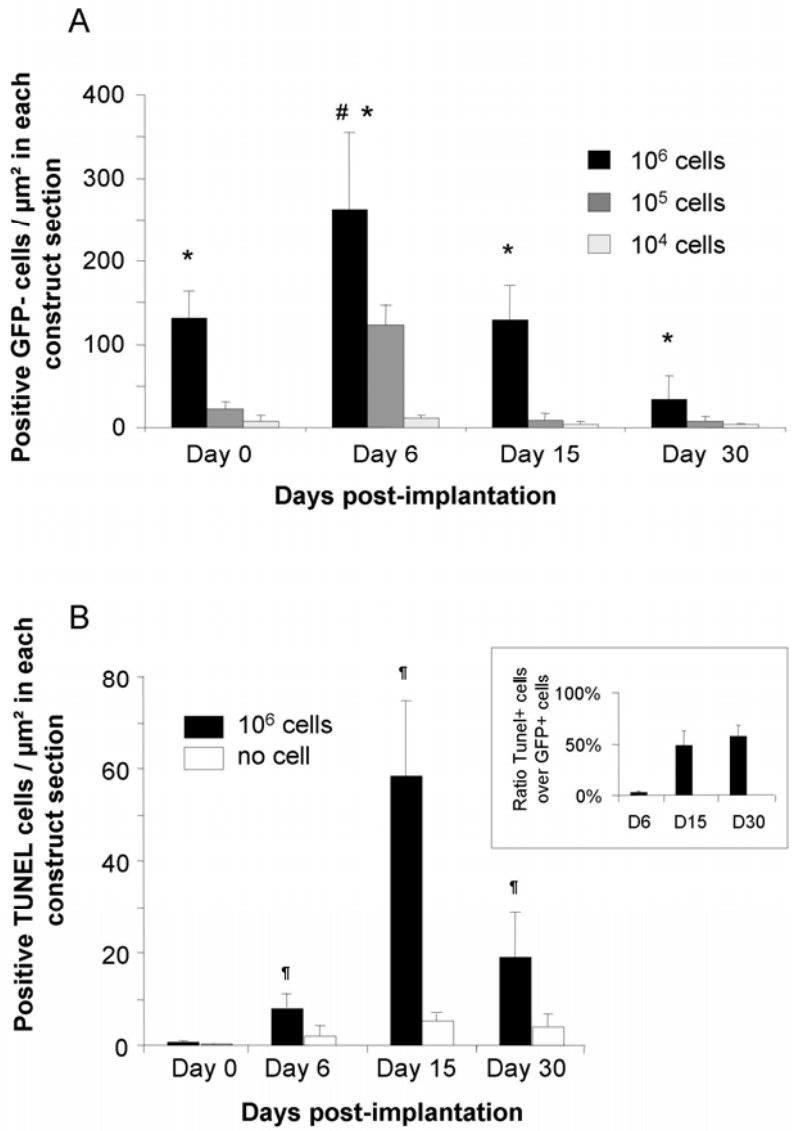

Figure 2: Anti-GFP and TUNEL staining confirmed the death of implanted hMSC. (A) Quantification of GFP positive cells per µm² detected per section from each cell construct either non-implanted (day 0) or explanted at different time points post-implantation. (B) Time course of TUNEL positive cells per µm² detected per section from either unseeded constructs (white bars) or constructs seeded with 1x106 cells (black bars). INSERT: Number of TUNEL-positive cells normalized to the number of GFP-positive cells detected on the same section from constructs seeded with 1x106 cells. Two stained sections from each construct were counted; n=5 constructs for each cell seeding density tested. The data were expressed as means ± SEM. * $p < 0.05$ for the constructs seeded with 1x106 cells compared to constructs seeded with other cell densities (Mann-Whitney test); # $p < 0.05$ for the constructs analyzed at day 6 post-implantation compared to those analyzed at other time points (Mann-Whitney test); ¶ $p < 0.05$ for the constructs seeded with 1x106 cells compared to unseeded constructs (Mann-Whitney test).

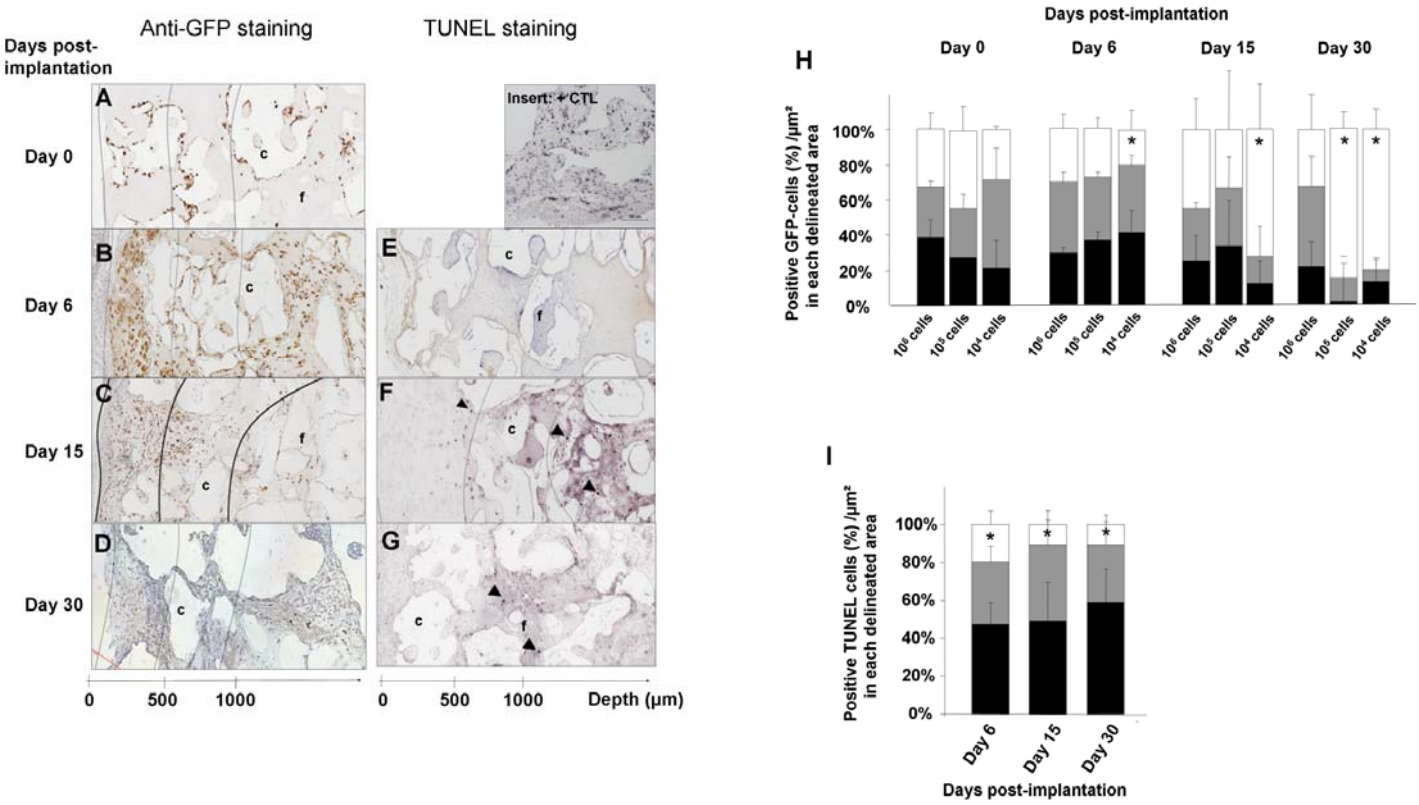

Figure 3: Histology analysis revealed that implanted hMSC in the inner part of the constructs died first. Sections from constructs seeded with 1x106 cells were labeled with anti-GFP immunostains (Frames A, B, C and D) and with TUNEL labeling (Frames E, F and G). These images show the implanted hMSC and apoptotic cell distribution (black arrow heads) throughout the construct sections. The black lines separate the different areas of depth in the constructs: specifically, outer (from 0 to 500 µm), in-between (from 500 to 1,000 µm) and inner (> 1,000 µm of depth). c = coral; f = fibrin. Insert: Sections treated with DNAse (positive control). (H) Percentage of GFP positive cells present in the outer (white bars), in-between (grey bars) and inner (black bars) areas delineated in each construct section. (I) Percentage of TUNEL-positive cells present in the outer (white bars), in-between (grey bars) and inner (black bars) in the delineated regions of the sections from constructs seeded with 1x106 cells. Two stained sections from each construct were examined; n=5 constructs for each cell-seeding density tested. The data were expressed as mean ± SEM. * $p < 0.05$ for the positive cells present in the outer area compared to positive cells present in the in-between and inner areas (Mann-Whitney test).

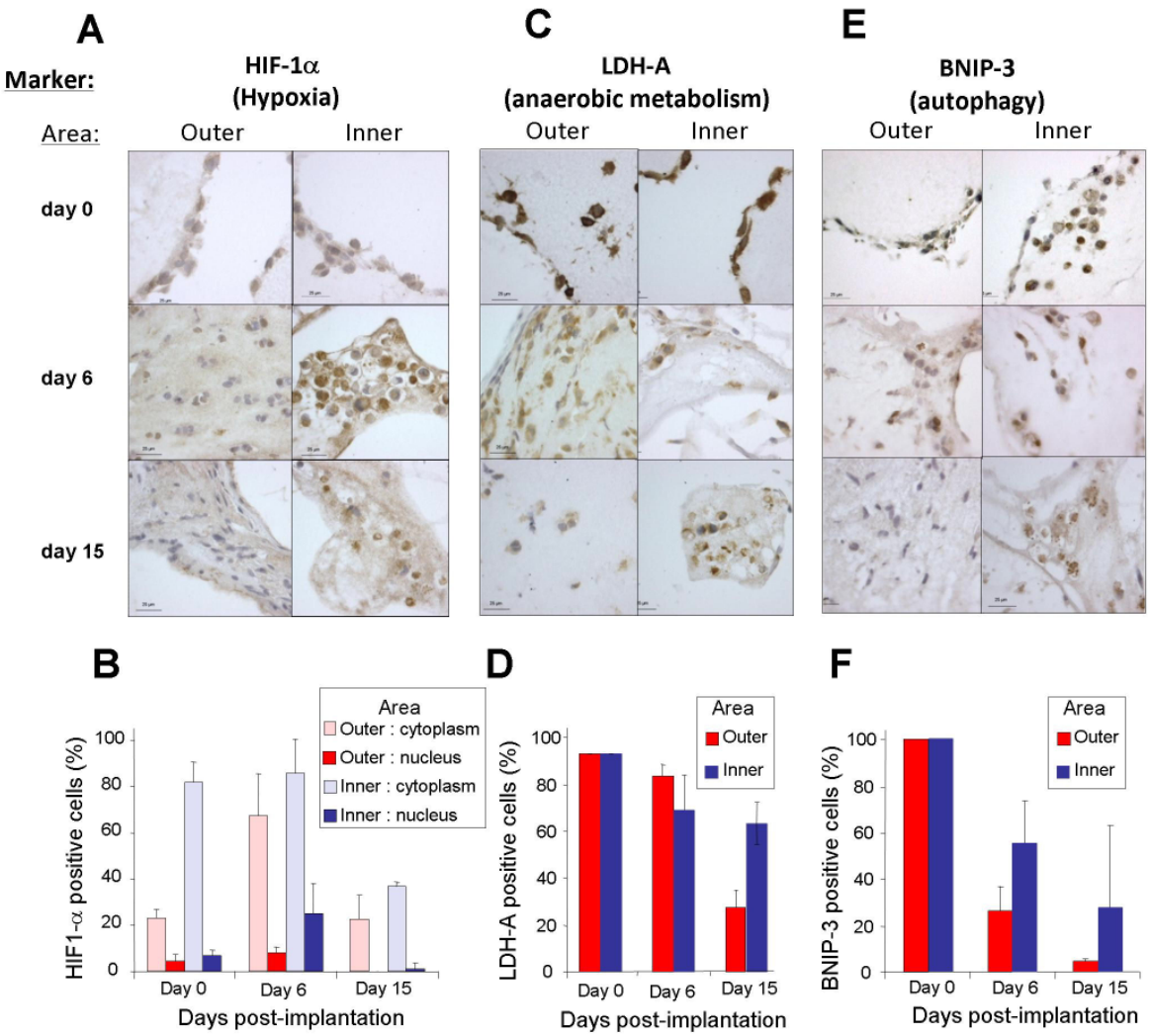

Figure 4: The hMSC within the constructs tested expressed ischemic markers. Sections of constructs seeded with 1x106 cells, either non-implanted (day 0) or implanted for 6 and 15 days, were immunostained for (A) HIF-1α, (C) LDH-A and (E) BNIP-3 proteins. Stained cells were visualized in either the outer (<500 µm of depth) or in the inner (>1,000 µm of depth) areas. The number of (B) HIF-1α, (D) LDH-A and (F) (BNIP-3) positive cells per field present in either the outer (red bars) or inner area (blue bars) of the constructs seeded with 1x106 cells were counted. HIF-1α positive cells stained at the cytoplasmic level and were distinguished from those cells stained at both the cytoplasmic (pink and light blue) and nuclear levels (dark red and dark blue). For each marker examined, the stained cells were counted in 5 fields from each area of each section (corresponding to more than 100 observed cells). The data were expressed as means ± SEM.

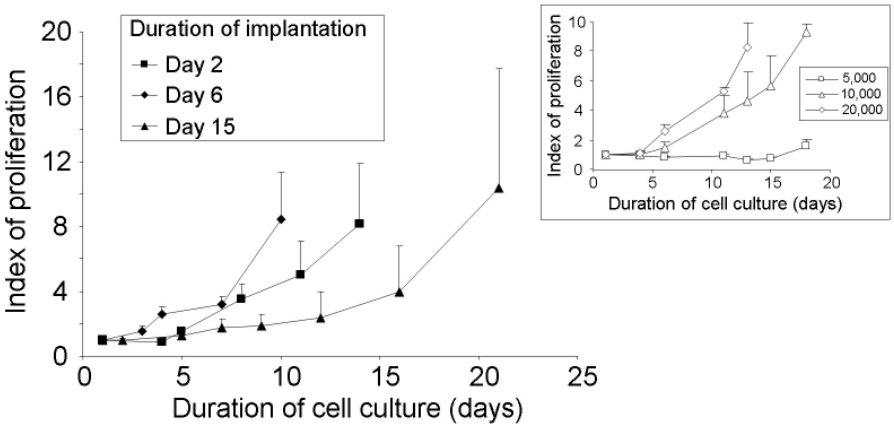

Figure 5: The hMSC present in the constructs tested remained viable for up to 15 days post-implantation. In vitro cell proliferation of Luc-GFP-hMSC extracted from constructs explanted 2, 6 and 15 days post-implantation was determined. Cell proliferation was monitored non-invasively using BLI after addition of luciferin substrate to the cell cultures. The "index of proliferation" was defined as the photon flux from the cells present in each well measured at each time point normalized to that measured at day 1 post-seeding. INSERT: Time course of in vitro cell proliferation of Luc-GFP-hMSC seeded at 5,000, 10,000 and 20,000 cells/cm². The data were expressed as means ± SEM; n=8 constructs for each duration of implantation tested and n= 3 for each cell-seeding density tested.

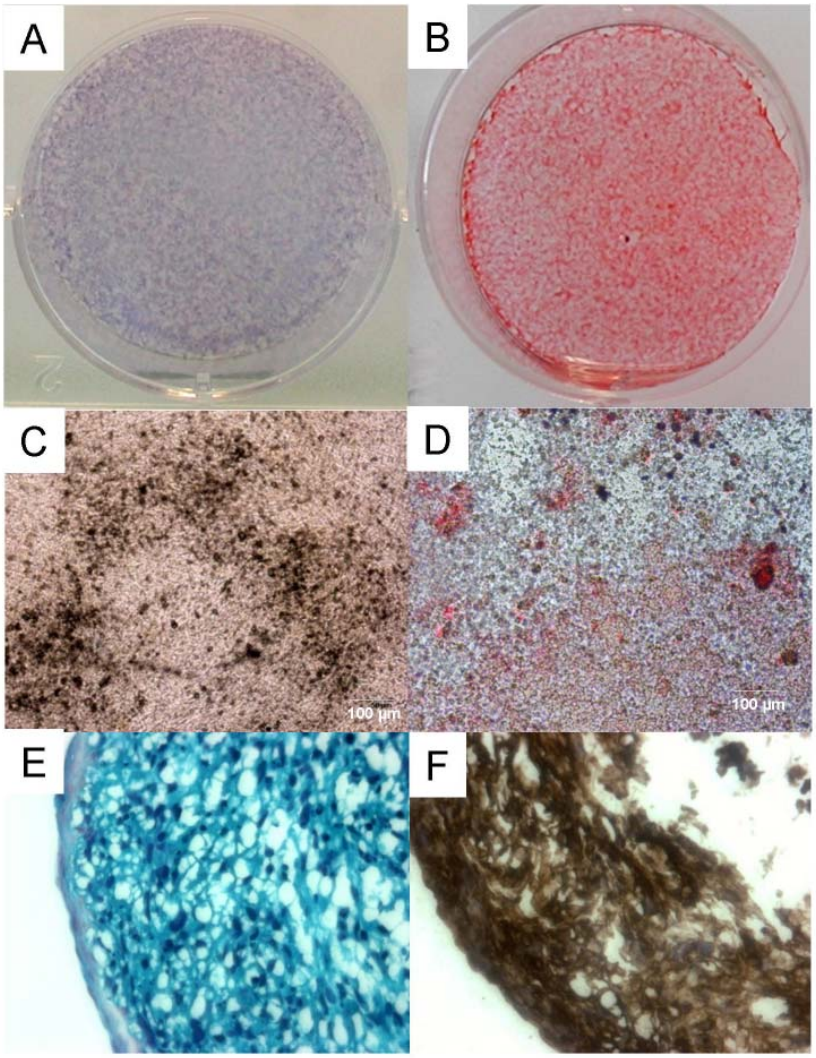

Supplementary Figure 1: Analysis of the multilineage potential of SV56-hMSCs following differentiation. For the osteogenic differentiation, the SV56 cells were seeded at a density of 6.103 cells/cm² in 6-well plates and cultured in αMEM medium containing 10% FCS, 10-7 M dexamethasone, 150 µM ascorbic acid-2 phosphate and 2 mM β-glycerophosphate for 21 days. At that time, the SV56 cells were stained to determine (A) alkaline phosphatase activity (Degat et al. J Biomed Mater Res 2009) and to detect matrix mineralization using (B) Alizarin red and (C) von Kossa stains (Quarto et al. Tissue Eng, 2006). For the adipogenic differentiation, cells were seeded at a density of 6.103 cells/cm² in 6-well plates and cultured in αMEM containing 10% FCS, 10-7 M dexamethasone, 0.5 mM IBMX, 5 µg/ml insulin, and 60 µM indomethacin for 21 days. At that time, the SV56 culture dishes were stained with Oil Red O (Zuk et al., Tissue Eng, 2001) to detect lipid accumulation. For the chondrogenic differentiation 5x104 SV56 cells were cultured in micromass pellets in the presence of high-glucose DMEM medium containing 50 µg/ml ascorbic acid-2 phosphate, 100 nM dexamethasone, 1% (v/v) ITS and 10 ng/ml TGFβ3 for 14 days (Mackay et al. Tissue eng, 1998). At that time, the SV56 cell aggregates were fixed, embedded in paraffin and processed for histochemical analysis; tissue sections were stained with (E) Alcian Blue, to detect sulfated proteoglycans, and (F) with anti-collagen type II immunostaining.

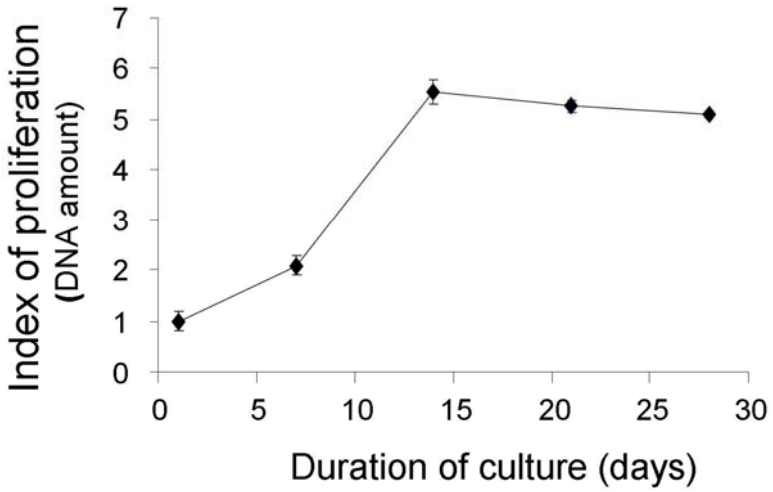

Supplementary Figure 2: Time course of SV56-hMSC proliferation onto coral scaffolds. SV56 cells were seeded onto the coral particles at the density of 10^5 cells/40 mg of particles in nonadhesive 24-well plates and cultured under standard cell culture conditions. At each time point, SV56/coral scaffolds were harvested and lysed by performing three freeze/thaw cycles; the DNA content was determined using the Picogreen dsDNA quantitation reagent (Molecular Probe). The "index of proliferation" was defined as the amount of DNA from the cells present in each sample quantified at each time point and normalized to the results obtained at day 1 post-seeding. Values are mean ± SEM n=3

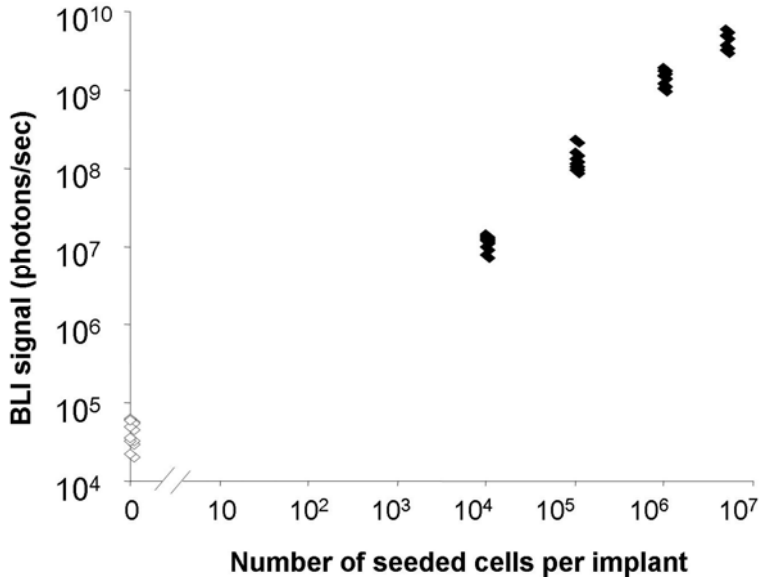

Supplementary Figure 3: In vitro BLI signals from fibrin gel/coral constructs either not seeded (white diamonds) or seeded with 1x10^4, 1x10^5, 1x10^6 or 5x10^6 hMSC-Luc-GFP (black diamonds). These results provided evidence for the efficacy of the cell seeding protocol used in the present study.

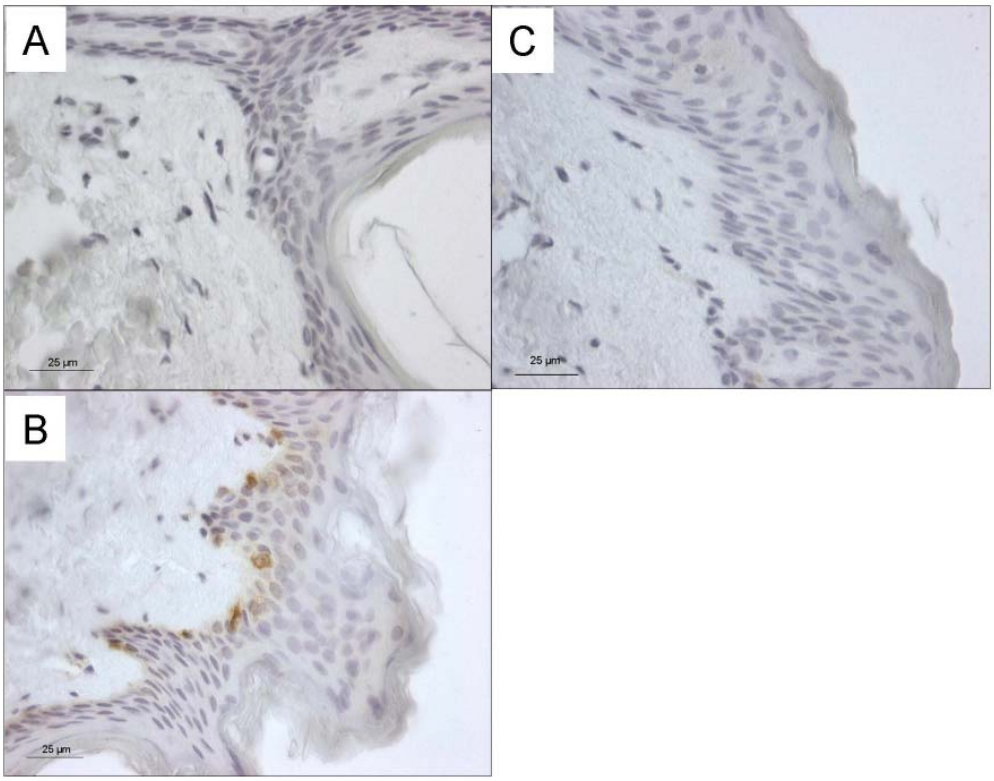

Supplementary Figure 4: Negative control stainings. Representative immunohistology results from human epidermis biopsies sections stained for the (A) HIF-1α, (B) LDH-A and (C) BNIP-3 (C) proteins. There was no staining for the HIF-1 and BNIP3 proteins on these specimens. Detection of the LDH-A protein in the basal layer was weak.

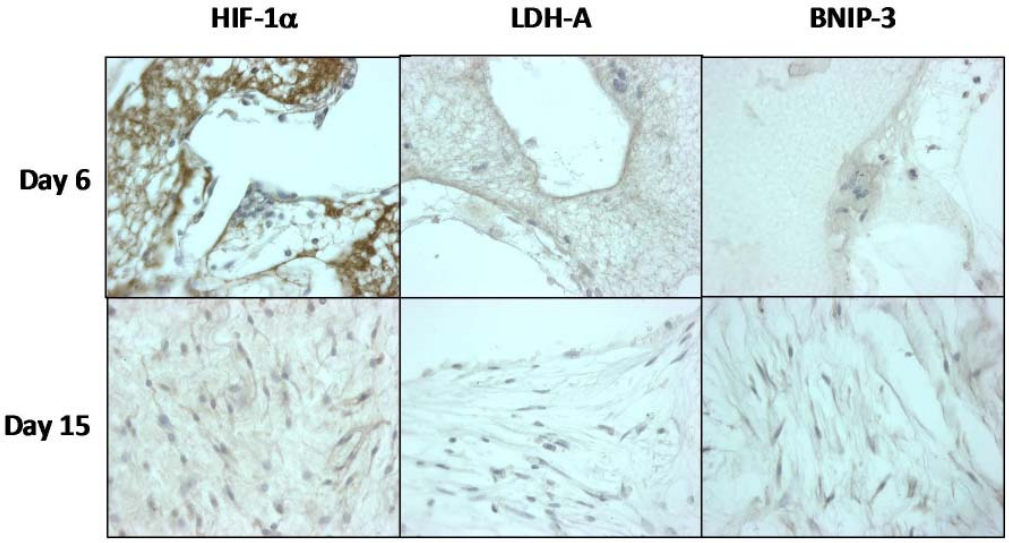

Supplementary Figure 5: Representative sections from non hMSC-seeded constructs (Control group) implanted for 6 and 15 days and stained for the HIF-1α, LDH-A and BNIP-3 proteins. There was no specific cell staining for the HIF-1α, LDHA, and for the BNIP3 proteins on these specimens providing evidence that the invading host cells did not express the ischemic markers. Note the strong non-specific staining of the fibrin gel with the anti-HIF-1α antibody on the section of the construct explanted at day 6 post-implantation.

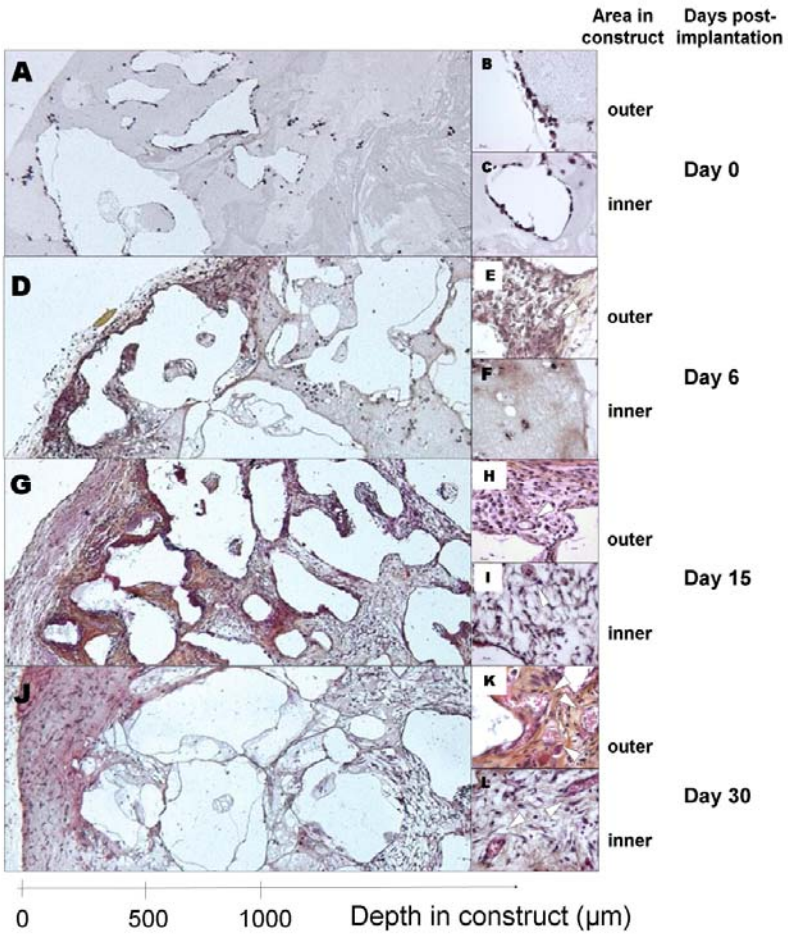

Supplementary Figure 6 : Representative HES results from sections of constructs seeded with 1x106 cells and either non-implanted (Frames A, B and C) or explanted at day 6 (Frames D, E and F), at day 15 (Frames G, H and I) and at day 30 (J, K and L) post-implantation. These results illustrate the progressive host tissue infiltration and new blood vessels (white arrow head) invasion from the periphery of the construct at day 6 (Frame E) and at day 15 (Frame H) towards the centre of the construct at day 15 (Frame I) and at day 30 (Frame L) post-implantation.